Sensitivity function-based Identification Of Solid Oxide Electrolyzer Parameters

Zaman Yazbeck, Federico Bribiesca Argomedo, Minh Tu Pham, Bertrand Morel, Ronit-Kumar Panda, Vincent Dimitriou

Sensitivity function-based Identification Of Solid Oxide Electrolyzer Parameters

Z. Yazbeck, F. Bribiesca-Argomedo, M.T. Pham, B. Morel, R.K. Panda, V. Dimitriou

***Abstract*— This paper presents a framework for parameter estimation of Solid Oxide Electrolyzer Stack (SOES) model. The complexity of multi-physics in SOES models poses a unique challenge for parameter identification due to the presence of nonlinearities, the large number of parameters, and few available measurements. Consequently, this study presents an enhanced method of parameter estimation, based on the Gauss-Newton optimization algorithm, incorporating a truncated Singular Value Decompostion (SVD) of a normalized sensitivity matrix. This modification prioritizes the update of parameters in the directions of high sensitivity while limiting the condition number of the matrix inverted to choose the step size, thus attenuating the adverse effects of noise and model errors unavoidable in the estimation process. This departure from the conventional approaches, allows a more nuanced and effective identification strategy tailored to the intricacies of SOESs. The proposed method is validated using data from an experimental test bench and compared to other identification methods.**

***Index Terms*— SOEC, electrochemical systems, parameter identification, sensitivity function, singular value decomposition, optimization.**

I. INTRODUCTION

Concerns related to climate change have increased in the past several years and necessitate the development and commercialization of alternative, renewable, and carbon-neutral energy production and storage technologies. Among the different possibilities, Solid Oxide Electrolyzer Cells (SOECs), or high-temperature electrolyzers, known for its ability to produce clean hydrogen without carbon emissions, can significantly contribute to the global transition away from fossil fuels [1]. To enhance efficiency, SOECs are often set up in a modular configuration to form a stack (SOES). However, the deployment of solid oxide cell systems in the market is still limited. This can be attributed to shortcomings related to the durability, reliability, and high cost of current versions [2]. Addressing these issues through advanced monitoring and diagnostics is crucial for enhancing the technology's reliability and efficiency, thus supporting its integration into the energy landscape.

In this context, mathematical models have become essential tools, yet require knowledge of multiple parameters that are often impossible to measure directly. The accuracy of these models depends on the adequate choice of these parameters, that are often fitted from experimental data. Therefore, the parameter identification problem is important for the development of reliable diagnostic methods for SOES systems.

Many mathematical models for Solid Oxide Cells (SOC) in fuel cell mode (SOFC) or electrolysis mode (SOEC) have been described in the literature, describing the balance laws and electrochemical behavior in zero-dimensional (or lumped-parameter) models [3], one-, two- or three-dimensional partial differential equation (PDE) models [4], [5] and [7]. These models are established mostly at the individual cell level and are scaled up in the case of a full stack by multiplying the cell voltage by the number of series-connected cells constituting the stack.

Most of the current literature on SOEC/SOFC parameter identification focuses on parameter fitting, specifically aligning the model outputs with experimental data. However, little work has been done to explore under which circumstances the experimental data is sufficiently rich to independently estimate all the parameters. For instance, in [8], the parameters of the electrochemical model for SOFC are estimated using an extensive set of experiments and applying the distribution of relaxation time method (DRT). In [9] and [10], an "all-in-one" strategy is used to fit more than ten parameters from experimental data, employing a non-linear curve fitting method and a genetic algorithm, respectively. This proliferation of parameters that require fitting is a common occurrence in electrochemical models, as evidenced in studies concerning battery systems or other types of fuel cells [12] .

In order to address the issue of parameter identifiability in battery models, the authors in [12] and [13] compute the sensitivity matrix of the outputs with respect to the different parameters. This matrix represents the local impact of parameter changes on the available measured outputs as a function of time. Using this information, a correlation matrix can be established along a trajectory (or an experimental run) in order to assess which parameter subsets can be independently identified and which produce similar variations in the outputs. Once the relative directions of sensitivity matrix have been established, it is possible to group and rank them manually based on their importance and impact on the output for a sequential parameter estimation as a final step.

Inspired by these results, this paper introduces a different approach for parameter estimation utilizing sensitivity equations that, instead of using manual clustering and *ad hoc* parameter choices for the identification process, uses a varia-

This work was supported by GENVIA and the Association Nationale de la Recherche et de la Technologie.

Z. Yazbeck, R.K. Panda, and V. Dimitriou are with GENVIA SAS, Plaine Saint Pierre, 34500 Béziers, France, zaman.yazbeck@genvia.com

Z. Yazbeck, F. Bribiesca-Argomedo and M.T. Pham are with INSA Lyon, Universite Claude Bernard Lyon 1, Ecole Centrale de Lyon, CNRS, Ampère, UMR5005, 69621 Villeurbanne, France,

Z. Yazbeck and B. Morel are with Univ. Grenoble Alpes, CEA/LITEN, 17 Avenue des Martyrs, 38054, Grenoble, France

tion of the Gauss-Newton algorithm and a truncated singular-value decomposition (SVD) to automate the improvement directions that are followed at every step. This automated process directs the optimization algorithm towards the most influential parameters, thereby enhancing efficiency, while imposing limits on the condition number of the linear system that is solved at each iteration of the optimization. This truncation is designed to alleviate the effects of measurement noise and prevent the algorithm from taking too large steps in directions where the sensitivity is particularly low. This has the advantage of avoiding non-physical parameter values and decreasing the estimated parameter variation when noise is present in the measurements.

This paper is structured as follows: Section II delves into SOEC technology and the electrolysis process; Section III outlines the proposed parameter identification method; Section IV presents the validation of the method using experimental data from a SOES system and a comparison to other identification methods. Finally, Section V presents the conclusions and future perspectives.

II. Stack dynamic model

A. SOEC technology

Solid Oxide Electrolyzer Cells (SOECs) split steam into hydrogen $H_{2_{(g)}}$ and oxygen $O_{2_{(g)}}$ gases at high temperatures ($700°C - 800°C$). This high-temperature operation partially replaces the need for electrical power by utilizing heat, improving the overall energy conversion efficiencies. High temperatures also accelerate chemical reactions, making the overall process more thermodynamically efficient. Essentially, SOECs use high temperatures to achieve more effective and efficient hydrogen production, capitalizing on both thermal and electrical energies for a more sustainable and cost-effective process.

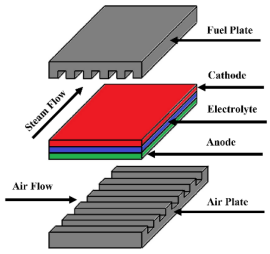

Fig. 1. Schematic of Cross-flow Single repeating Unit [6] (at the cell level).

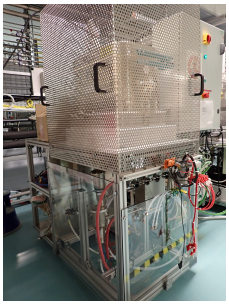

Fig. 2. Studied test bench (at the system level).

As shown in Fig. 1, the Solid Oxide Electrolyzer Cells (SOECs) are comprised of three key components: the electrodes, the electrolyte, and the interconnect plates [6]. The electrodes, which include an anode and a cathode, play a crucial role in facilitating the electrochemical reactions (1). In particular, water molecules are first reduced in the cathode to form Hydrogen gas and charged oxygen ions. These ions are transported through the electrolyte, mainly due to diffusion and electric potential differences, and then oxidized on the Anode to form Oxygen gas [5]. Additionally, electrical connections on both sides of the cell are required to close the circuit so that the electronic exchange (i.e. current flow) can be maintained

$$Cathode: \quad H_2O_{(g)} + 2e^- \rightarrow H_{2_{(g)}} + O^{2-} \tag{1a}$$

$$Anode: \quad O^{2-} \rightarrow \frac{1}{2}O_{2_{(g)}} + 2e^- \tag{1b}$$

$$Overall: \quad H_2O_{(g)} \rightarrow \frac{1}{2}O_{2_{(g)}} + H_{2_{(g)}} \tag{1c}$$

In this paper, a dynamic model is developed for a cell, also called *single repeatable unit* (SRU), and then scaled up to the stack level by assuming a uniform behavior across all units. The model integrates energy balance equations, reaction kinetic models, and mass transport models, that will be detailed in the next subsections. Additionally, Ohm's law is applied to account for the electrical conductivity and resistance variation within the cell, with assumptions based on ideal gas behavior due to the high operational temperatures [14]. Given the SOEC operation at atmospheric pressure, the model is simplified by neglecting the pressure drop across the air and fuel compartments.

B. Thermal Balance equation:

In our model, the energy balance equation is simplified by assuming the air outlet temperature is representative of the overall stack temperature, consolidating the anode and cathode temperatures into a single value, denoted T_s. The mass balance equation is represented by the relation [4]:

$$K_{stack}\frac{dT_s}{dt} = \dot{E}^{in} - \dot{E}^{out} + IV_s - \Delta\hat{H}_r + Q^{conv} \tag{2}$$

where K_{stack} is the stack lumped heat capacity, $\Delta\hat{H}_r$ is the enthalpy of formation, V_s is stack voltage, I is the current applied to the stack, and $\dot{E}^{in}$ and $\dot{E}^{out}$ denote the energy flows in and out of the stack respectively, further decomposed as:

$$\dot{E}^{\alpha} = \dot{N}_j^{\alpha}\sum_i y_i^{\alpha} h_i(T_j^{\alpha}) \tag{3}$$

were, y_i^{α} represents the molar fraction of the ith gas component, $i \in \{H_2, H_2O, O_2, N_2\}$ with its corresponding molar flow rate $\dot{N}_j$, where $j \in \{fuel, air\}$, at the respective locations indicated by $\alpha \in \{in, out\}$. The temperatures at these locations are denoted by T_j^{α}, and h_i represents the enthalpy of the gases, calculated using from the NIST data tables [15]. The term Q^{conv} in (2) encompasses the convective heat exchange occurring among the air, fuel, furnace, and stack:

$$\begin{aligned} Q^{conv} = {} & h_{air,stack}^{conv}(T_{air}^{in} - T_s) + h_{fuel,stack}^{conv}(T_{fuel}^{in} - T_s) \\ & + h_{oven,stack}^{conv}(T_{oven} - T_s) \end{aligned} \tag{4}$$

Where $h_{j,stack}^{conv}$ and $h_{oven,stack}^{conv}$ are the convective heat coefficients, were fitted from experimental data.

C. Mass balance

According to the law of conservation of mass, the expression for the molar fraction (y_i) of component i in the channels is given by:

$$\frac{PV_{ch}}{RT_s}\frac{dy_i}{dt} = \dot{N}_j^{in} y_i^{in} - \dot{N}_j^{out} y_i^{out} + r_i \tag{5}$$

for $i \in \{H_2, H_2O, O_2\}$, $j = \{fuel, air\}$, where V_{ch} is the volume of the of the fluids inside the channels, P is the pressure of the fluids in Pascals (Pa), R is the gas constant equal to 8.314 $J/(molK)$, and r_i represents the produced/consumed flows described according to Faraday's law as:

$$r_{H_2} = -r_{H_2O} = 2r_{O_2} = \frac{I}{2F} \tag{6}$$

Where F is the Faraday constant. The output flow rate for the fuel and air side is calculated as follows:

$$\dot{N}_j^{out} = \dot{N}_j^{in} + \sum r_i \tag{7}$$

D. Electrochemical model

The stack voltage V_s is given by the cell voltage, V_{cell}, multiplied by the number of cells in the stack, N_{cell}, as follows:

$$V_s = N_{cell} V_{cell} = N_{cell}(V_{nernst} + \eta_{ohm} + \eta_{act} + \eta_{conc}) \tag{8}$$

where η_{ohm}, η_{act}, η_{conc} represent ohmic, activation, and concentration overpotential, respectively.
The reversible thermodynamic voltage is:

$$V_{nernst} = E^0(T_s) + \frac{RT_s}{2F} \ln\left(\frac{y_{H_2} y_{O_2}^{0.5}}{y_{H_2O}}\right) \tag{9}$$

Where E^0 refers to the Gibbs free-energy change of the reaction.

1) Ohmic resistance: is the voltage loss due to resistance to the flow of electrons through electrodes and interconnections and the flow of ions through the electrolyte. It is as follows E_{act}^{ohm}:

$$\eta_{ohm} = IR_s exp\left(\frac{E_{act}^{ohm}}{R}\frac{1}{T_s}\right) \tag{10}$$

Where R_s is the electrolyte resistance and E_{act}^{ohm} is the activation energy for ion transport. These parameters are fitted from the experimental data [16].

2) Activation Overpotential: is the energy required to overcome the reaction barriers at the electrodes, and it is determined using the Butler-Volmer equations [18].

$$\eta_{act} = \frac{RT_s}{F}\left[\sinh^{-1}\left(\frac{I}{2I_{0,an}}\right) + \sinh^{-1}\left(\frac{I}{2I_{0,cath}}\right)\right] \tag{11}$$

Where the exchange current densities for anode and cathode $I_{0,an}$ and $I_{0,cath}$ follow the Arrhenius's law [5]:

$$I_{0,cath} = \gamma_{cath} y_{H_2}^{\zeta} y_{H_2O}^{\theta} \exp\left(-\frac{E_{act}^{cath}}{RT_s}\right) \tag{12}$$

$$I_{0,an} = \gamma_{an} y_{O_2}^{\kappa} exp \exp\left(-\frac{E_{act}^{an}}{RT_s}\right) \tag{13}$$

The exponents ζ, θ, and κ are fixed to be equal to 0.066, 0.81, and 0.15 respectively according to [17]. While γ_{an} and γ_{ca} and the activation energies for corresponding reactions, E_{act}^{an} and E_{act}^{cath}, are identified from experimental data.

3) Concentration Overpotential: arises due to the drastic reduction in the concentration of the reactants at the electrodes [5], [16].

$$\eta_{conc} = \frac{RT_s}{2F} \ln\left(\frac{y_{H_2,TPB} y_{H_2O}}{y_{H_2} y_{H_2O,TPB}}\right) + \frac{RT_s}{4F} \ln\left(\frac{y_{O_2,TPB}}{y_{O_2}}\right) \tag{14}$$

$$y_{H_2O,TPB} = y_{H_2O} - \frac{RT_s}{2F}\frac{d_{cath}}{D_{H_2O,H_2}^{eff} P_{fuel}} I \tag{15}$$

$$y_{O_2,TPB} = 1 + (y_{O_2} - 1) exp\left(-\frac{RT_s}{4F}\frac{d_{an}}{D_{O_2,N_2}^{eff} P_{air}} I\right) \tag{16}$$

Where $y_{i,TPB}$ is the partial pressures of the specie i at the interface electrode/electrolyte, d_i is the thickness of the electrodes - anode or cathode, and $D_{i,j}^{eff}$ is the effective diffusion coefficient [5] - [19].

E. State-space formulation

All the equations above are presented in state-space form as follows:

- The state vector $x = [y_{H_2}\ y_{H_2O}\ y_{O_2}\ T_s]^T$:

$$\begin{cases} \dot{y}_{H_2} &= \frac{RT_s}{PV_{ch}}(\dot{N}_{fuel}^{in} y_{H_2}^{in} - \dot{N}_{fuel}^{out} y_{H_2}^{out} + \frac{I}{2F}), \\ \dot{y}_{H_2O} &= \frac{RT_s}{PV_{ch}}(\dot{N}_{fuel}^{in} y_{H_2O}^{in} - \dot{N}_{fuel}^{out} y_{H_2O}^{out} - \frac{I}{2F}) \\ \dot{y}_{O_2} &= \frac{RT_s}{PV_{ch}}(\dot{N}_{air}^{in} y_{O_2}^{in} - \dot{N}_{air}^{out} y_{O_2}^{out} + \frac{I}{4F}) \\ \dot{T}_s &= \Big[(y_{H_2}^{in} h_{H_2}(T_{fuel}^{in}) + y_{H_2O}^{in} h_{H_2O}(T_{fuel}^{in}))\dot{N}_{fuel}^{in} \\ &\quad + (y_{O_2}^{in} h_{O_2}(T_{air}^{in}) + y_{N_2}^{in} h_{N_2}(T_{air}^{in}))\dot{N}_{air}^{in} \\ &\quad - (y_{H_2}^{out} h_{H_2}(T_s) + y_{H_2O}^{out} h_{H_2O}(T_s))\dot{N}_{fuel}^{out} \\ &\quad - (y_{O_2}^{in} h_{O_2}(T_s) + y_{N_2}^{in} h_{N_2}(T_s))\dot{N}_{air}^{out} \\ &\quad + IV_s + Q^{conv}(T_s) - r_{H_2}\Delta\hat{H}_r(T_s)\Big]/K_{stack} \end{cases} \tag{17}$$

- The controllable inputs are:

$$u = [I\ \dot{N}_{fuel}^{in}\ \dot{N}_{air}^{in}\ y_{H_2}^{in}\ y_{H_2O}^{in}\ T_{fuel}^{in}\ T_{air}^{in}\ T_{oven}]^T \tag{18}$$

- The measured output Y:

$$Y = V_s(x, u, \lambda) \tag{19}$$

Where V_s is defined in (8), and λ is the vector of unknown parameters that need to be fitted using experimental data:

$$\lambda_{elech} = [R_s\ E_{act}^{ohm}\ \gamma_{an}\ \gamma_{cath}\ E_{act}^{an}\ E_{act}^{cath}]^T$$

$$\lambda_{thermal} = [K_{stack}\ h_{conv}^{air,stack}\ h_{conv}^{fuel,stack}\ h_{conv}^{oven,stack}]^T$$

$$\lambda = [\lambda_{elech}^T\ \lambda_{thermal}^T]^T$$

Parameters	R_s	$E_{act}^{ohm/an/cath}$	$\gamma_{an/cath}$	K_{stack}	$h_{conv}^{air,stack}$
Units	KJ/mol	A/cm^2	$\Omega \cdot cm^2$	J/K	W/K

TABLE I
PHYSICAL PARAMETERS AND THEIR UNITS

Even though in this paper we consider four thermal (λ_{therm}) and six electrochemical (λ_{elech}) parameters (see Table I), other models may include even more parameters. For instance [9]-[10], has a model requiring 13 parameters. In this work, we fixed the exponents ζ, θ, and κ from the literature [17], in order to slightly reduce the complexity of the parameter identification process [5].

From the state space equations (17), it can be seen that the identification problem is nonlinear. Additionally, the challenge is compounded by the presence of a substantial number of physical parameters requiring identification and a reduced number of available measurements. To address this issue, constrained nonlinear identification techniques offer a potential solution. However, employing such methodologies may result in solutions where some identified parameters saturate at the predefined physical boundaries set by the user. This raises the question of whether these parameters are identifiable along the considered excitation trajectory and whether prioritizing their selection over direct identification efforts is advisable. In the subsequent section, we will introduce a systematic approach for parameter estimation, utilizing a modified algorithm of the Gauss-Newton method.

III. Parameter identification framework

In this section, the fundamental theory for sensitivity analysis in the optimization problem, which forms the basis of this work, is presented explaining the framework employed for the parameter estimation algorithm.

A. Sensitivity function-based identification algorithm

In the literature, the vast majority of methods estimate all necessary parameters from available experimental data. Nevertheless, depending on the specific trajectories of the nonlinear system, not all the outputs are necessarily sensitive with respect to variations of all parameters. Ignoring this information in the estimation process will induce significant estimation errors due to measurement noises or outliers [11] and give inaccurate, and unreliable estimations. By incorporating the sensitivity of output to parameters into the optimization algorithm, the parameter estimation process can be improved. This method directs the search towards the most sensitive parameter directions, minimizing the impact of measurement noise. Sensitivity measures how output dependency on parameter values changes with specific input trajectories.

1) Sensitivity differential equations: From the equations presented in Section II, we can present the model as an ordinary differential system of equations (ODEs) with the following form:

$$\begin{cases} \dot{x} = f(x, \lambda, u) \\ Y = h(x, \lambda, u) \end{cases} \tag{20}$$

Denote $x \in \mathbb{R}^4$ is the state vector, $Y \in \mathbb{R}^1$ is the measured output (19), $u \in \mathbb{R}^8$ is the control input (18), and $\lambda \in \mathbb{R}^{n_p}$ is the vector of parameters which we want to identify, where $n_p = 10$ is the number of parameters.

The local sensitivities are defined as the first-order partial derivatives of the states/output with respect to the parameters. Where $S_x^t(\lambda,t) = \dfrac{\partial x}{\partial \lambda}(\lambda,t) \in \mathbb{R}^{4\times n_p}$, and $S_y^t(\lambda,t) = \dfrac{\partial Y}{\partial \lambda}(\lambda,t) \in \mathbb{R}^{1\times n_p}$ are the sensitivity matrices, defined for each time t.

We used the sensitivity differential equations presenting the evolution of the sensitivity variables in time, as in [12], [21]. Thus we augment the number of ODEs and we calculate at each time step, in addition to the integration of the states, the sensitivity matrices:

$$\begin{cases} \dot{S}_x = \dfrac{\partial f}{\partial x} S_x + \dfrac{\partial f}{\partial \lambda} \\ S_y = \dfrac{\partial h}{\partial x} S_x + \dfrac{\partial h}{\partial \lambda} \end{cases} \tag{21}$$

The Jacobians in (21) can be numerically calculated. However, to address potential issues such as step size selection or the choice of finite difference method when numerically calculating the Jacobians in (21), we opted for an alternative approach. Specifically, rather than deriving the Jacobians by hand, we utilized a symbolic framework to compute them analytically. In this work, we employed CasADi [22] for efficient Jacobian calculations and used the IDAS integrator provided by SUNDIALS [23] for integration.

B. Parameter identification algorithm

For a single parameter, let us define an error trajectory as the difference between the predicted and experimentally measured values of the outputs in our system, evaluated at available time steps:

$$\varepsilon(\lambda) = V_s(\lambda) - V^{exp} \tag{22}$$

where the length of the vector ε corresponds to the number of time samples. We can then define an objective function to minimize as (half) the sum of the squared values of the error:

$$J = \frac{1}{2}\varepsilon(\lambda)^T \varepsilon(\lambda) \tag{23}$$

The first-order partial derivative of J with respect to the parameter vector λ is as follows:

$$\frac{\partial J}{\partial \lambda} = \varepsilon(\lambda)^T \frac{\partial \varepsilon(\lambda)}{\partial \lambda} = \varepsilon(\lambda)^T \frac{\partial Y}{\partial \lambda} = \sum_t \varepsilon_t(\lambda) S_y^t(\lambda,t) \tag{24}$$

The Gauss-Newton method uses a first-order Taylor expansion of the cost function to have the following iteration of the parameters [24]:

$$\begin{aligned} \lambda_{k+1} &= \lambda_k - \beta_k \left(\frac{\partial J}{\partial \lambda}^T \bigg|_k \frac{\partial J}{\partial \lambda}\bigg|_k \right)^{-1} \frac{\partial J}{\partial \lambda}^T \bigg|_k \varepsilon(\lambda_k) \\ &= \lambda_k - \beta_k S_y^{\dagger} \varepsilon(\lambda_k) \end{aligned} \tag{25}$$

Where $S_y^{\dagger}$ is the pseudo-inverse of the concatenation of the values of S_y^t for all time steps. For notational compactness, in the rest of this paper, we will use the notation $S_y \in \mathbb{R}^{n_T \times n_p}$ to refer to the full concatenation of S_y^t values for each time step (n_t being the number of time steps). Furthermore,

the parameter β_k, allows for the adaptation of the step-size at each iteration using a simplified line search technique [24]. It is essential to tune this parameter properly to have faster convergence and to converge to the local minima. The importance of β_k parameter will be discussed in the next section.

Due to the difference in orders of magnitude between the different parameters and outputs, a normalization of S_y is important:

$$S_{y,nrm} = S_y \Gamma \tag{26}$$

Where $\Gamma = diag(\frac{\lambda_1}{\|Y\|}, \ldots, \frac{\lambda_p}{\|Y\|})$ is a diagonal weighting matrix chosen as a function of the order of magnitude of each parameter divided by the order of magnitude of the output.

Afterwards, a truncation of the matrix $S^{\dagger}_{y,nrm}$ using a singular value decomposition (SVD) with a threshold value is used to avoid considering evolution directions with low sensitivities or ill-conditioned matrices in the pseudo-inverse computation in (25). This also limits the sensitivity of the steps with respect to small measurement errors or noise. Instead of using fixed *a priori* knowledge of linear dependence between the output sensitivity to different parameters (which is not always the same for a nonlinear system) for all iterations, we instead use a different truncation of $S^{\dagger}_{y}$ for each time-step using the following threshold:

$$\sigma_{thr} = max\{\sigma_{1,1} \times TOL_{rel},\ TOL_{abs}\} \tag{27}$$

Where the singular values that are smaller than σ_{thr} are treated as zeros during the computation of the pseudo-inverse matrix. $\sigma_{1,1}$ is the first and higher singular value, and the relative and absolute thresholds ($TOL_{rel} = 10^{-4}$ and $TOL_{abs} = 10^{-1}$, respectively) are selected to keep high singular values in each iteration, thus high sensitivities. The value of TOL_{rel} is related to the condition number of the sensitivity matrix, controlling how ill-conditioned the matrix is during inversion. While TOL_{rel} aims to prevent the algorithm from giving too much importance to small singular values, which could amplify numerical errors. On the other hand, TOL_{abs} is introduced to handle situations where the parameters exhibit a lack of sensitivity, ensuring that directions with very low sensitivity are not considered in the pseudo-inverse computation. This truncated version of the sensitivity matrix is used in the computation of the required pseudo-inverse in (25).

The pseudo-code of the proposed identification approach is presented in Algorithm 1.

C. Initial Guess

Since the problem is highly nonlinear, the selection of the initial guess plays a key role in preventing the optimization process from converging to local minima. For this reason, the initial guesses used for the electrochemical parameters (λ_{elec}) are based on :

- The impedance measurements at high frequency for the ohmic resistance parameters in (10) [20].
- Based on the literature for the other parameters related to the activation overpotential [5]-[20].

Algorithm 1 Sensitivity function-based parameter identification

Input: Experimental data, initial guess λ_0, β_0 TOL_{rel}, and TOL_{abs}, N

Output: Identified $\tilde{\lambda}$

Initialize: $\lambda \leftarrow \lambda_0$, $\beta \leftarrow \beta_0$, N
for $k = 1, 2, \ldots N$ **do**
  for $t = t_1, \ldots, t_{end}$ **do**
    $x_k = F(x_{k-1},\ \lambda_k,\ u_{k-1})$ ▷ F is the discretized function of f
    $Y_k = h(x_k,\ \lambda_k,\ u_{k-1})$
    $S_{x_k},\ S_{y_k}$
  end for
  $\varepsilon_k\ =\ Y_k - Y^{exp}$
  $S_{y_k,nrm} = S_{y_k} \times \Gamma$ ▷ Normalize S_{y_k}
  $USV^T = svd(S_{y_k,nrm})$
  $S_{y,r} = US_rV^T$ ▷ S_r is the truncation of S
  $\partial\lambda_k\ =\ -\beta_k(S_{y,r})^{\dagger}\varepsilon_k$ ▷ β_k is updated with a line search technique
  $\lambda_{k+1} \leftarrow \lambda_k + \Gamma^{-1}\delta\lambda_k$
end for

However, for the thermal parameters $\lambda_{thermal}$, the initial guess is put based on the geometries and materials of the stack.

IV. Experimental validation and Discussion

In this section, the modified sensitivity function-based Gauss-Newton method given in Algorithm 1, is applied to identify the parameter vector λ using experimental data. The data was obtained from the test bench in Fig. 2 with N_{cells} in the stack, which are cathode-supported cells, where each cell is instrumented to record its voltage.

Electrochemical Impedance Spectroscopy (EIS), was conducted on the stack shown in the Fig. 2. Additionally, various sensors measure the inlet temperature and pressure of the fuel and air, the voltage across each cell, the inlet flow rates of the gases, and the outlet flow rate of the produced hydrogen.

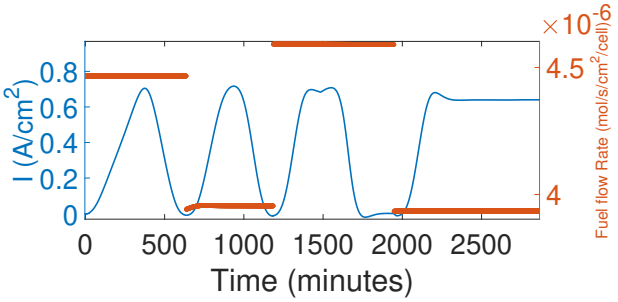

Fig. 3. Current density and Fuel flow rate inputs.

Different $I-V$ curves at different fuel flow rates, with the same inlet gas composition are applied during tests, as in Fig. 3, to assess performance losses under varying current conditions, aiding in the parameter fitting process.

Taking the initial guess defined in subsection C of the previous section, the algorithm takes around 150 iterations to converge to a 1.45 mean square error with an adaptive β, and more than 200 iterations when using fixed β as shown in Fig. 4.

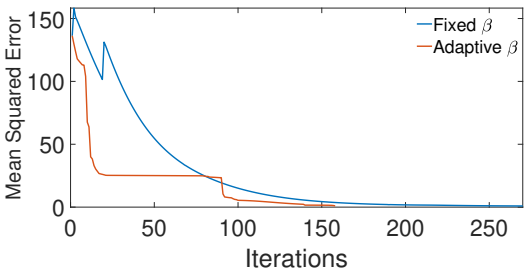

Fig. 4. Cost of objective function based on Sensitivity function-based with a fixed and adaptive step.

Figure 4 shows the importance of tuning and adapting β in each iteration. In fact, choosing a very small and fixed value of β is computationally very expensive. Conversely, choosing a bigger fixed value of β will increase the cost function for some iterations as in Fig. 4, potentially resulting in overshooting local minima or, in some cases, in divergence of the algorithm.

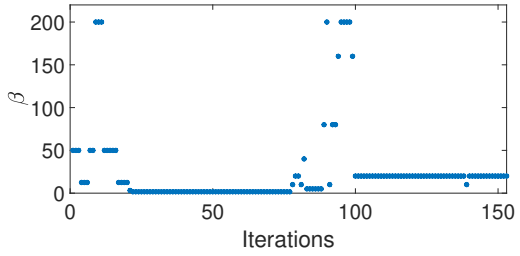

Fig. 5. Evolution of β, using the adaptive step approach in Fig.4.

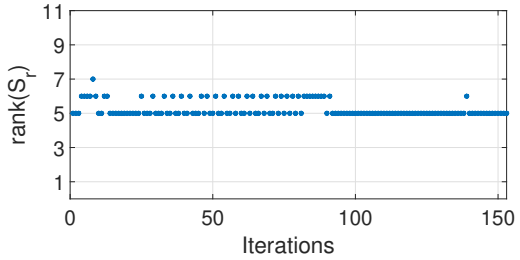

Fig. 6. Number of directions taken into account in each iteration.

Consequently, updating β in each iteration is essential to keep the cost function decreasing monotonically, as shown in Fig. 5 where the values of β are illustrated in each iteration. In the line search algorithm that we used, a maximum limit of β is put equal to 200.

As mentioned before, the truncation of the sensitivity matrix S_y is the main feature of the proposed approach. This enables the algorithm to choose the parameter update

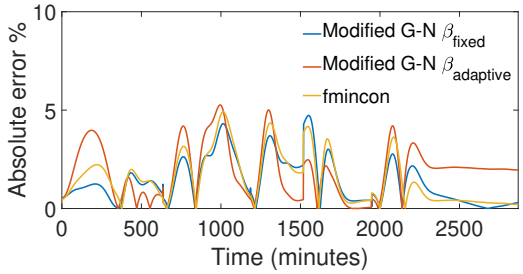

Fig. 7. Absolute voltage error between the simulated and experimental voltage with different optimizers: $100\frac{|Vs-Vexp|}{Vexp}$

direction only in those directions that are associated to large singular values while computing the pseudo-inverse in (25). To show the automated selection of descent directions, Fig. 6 shows that the rank of the corresponding truncated sensitivity matrix. This corresponds to the number of linearly independent directions used to explore and search for a solution to λ at each step of the modified Gauss-Newton method. It can be seen that the algorithm does not use the same number of directions at each iteration.

Table II presents the value of parameters which are the initial guess (I.G. column), the solutions of the modified Gauss-Newton algorithm with an adaptive (Adaptive β column) and fixed step β (Fixed β column) respectively with the classical Gauss-Newton iteration (G-N column) without truncation and normalization of the sensitivity matrix, a nonlinear optimization algorithm (fmincon column). All the methods used the same initial condition. Using these values, the absolute relative error of the voltage output is presented in Fig. 7.

It is important to emphasize that when using the classical Gauss-Newton iteration, the code breaks after two iterations. This termination occurs because some of the parameters calculated take negative values appearing inside logarithms (which have no physical interpretation, as presented in the column before the last in Table II). This happens despite the choice of a small step size β and is related to low sensitivity directions in the parameter space.

Parameters	I.G.	Adaptive β	Fixed β	G-N	fmincon
R_s	0.17	0.1403	0.34	-977.13	0.37
E_{act}^{ohm}	130	155	95	$165e3$	79
E_{act}^{an}	83	65	50	$-404e5$	$10.5e-3$
E_{act}^{cath}	159	85	56	114	91
γ_{an}	$4.2e4$	$4.37e4$	$4.3e4$	$3.88e12$	$6.3e4$
γ_{cath}	$2.76e6$	$2.4e4$	$5e6$	$-1.14e7$	$2.7e6$
K_{stack}	20	24.8	3.03	95.8	$1.9e4$
$h_{conv}^{air,stack}$	1.8	2.6	1.9	173.7	$1.09e5$
$h_{conv}^{fuel,stack}$	41.52	30	41.6	122.06	$2.76e4$
$h_{conv}^{oven,stack}$	146.7	137.8813	64	784	$2e5$

TABLE II

PARAMETER VALUES WITH THE CLASSICAL, MODIFIED GAUSS-NEWTON TECHNIQUE WITH ADAPTIVE AND FIXED STEP SIZE, AND FMINCON.

A comparison is also made with 'fmincon', one of the well-known constrained (local) optimization algorithms in MATLAB. Here we have imposed positivity of all parameters to avoid the issue encountered with the Gauss-Newton algorithm previously: Despite this positivity constraint, the parameters found with fmincon use the local information of cost decrease in all directions (including those of low sensitivity) and give parameters that are less physically meaningful than those obtained with the proposed method. It can be seen that several of them are far from the expected orders of magnitude (illustrated by the initial guess).

Fig. 7 shows the voltage behaviors from the calibrated model using a different dataset than that used in the optimization. The proposed method gives error values comparable to those obtained with 'fmincon', yet the physical meaning of the parameters is retained. Furthermore, the step adaptation strategy also shows similar levels of error after roughly half the number of iterations as the fixed-step method. It ensures that the algorithm does not diverge if the cost function is too flat (analogous to the problems that appear when using the Gauss-Newton method).

V. CONCLUSIONS AND FUTURE WORKS

A. Conclusions

In this paper, we have presented an extension of the Gauss-Newton method for systematically identifying electrochemical parameters in a Solid Oxide Electrolyzer (SOEC) model. The approach uses the output sensitivity information, quantifying how parameter variations impact the model outputs. This information is derived from the sensitivity differential equation through a symbolic framework and is then exploited using a truncated singular value decomposition in order to iteratively update the parameter estimates. This approach is validated using experimental data, demonstrating convergence to a solution consistent with the literature and expected trends and significantly reduces the square error of the model. While the physical significance of the solution cannot be definitively confirmed due to the lack of knowledge of actual parameters, the results indicate that the method provides a reliable fit within the given model framework. Furthermore, the proposed approach is compared to a standard Gauss-Newton method and the Matlab 'fmincon' function.

B. Future Works

Future work will focus on improving the accuracy and reliability of parameter estimation by incorporating confidence intervals to quantify the uncertainty in the estimates. This will enhance the robustness of the model and provide a more solid foundation for subsequent tasks such as fault detection, diagnosis, and prognosis.

REFERENCES

[1] A. Hauch, R. Küngas, P. Blennow, A.B. Hansen, J.B. Hansen, B.V. Mathiesen, and M.B. Mogensen, "Recent advances in solid oxide cell technology for electrolysis", *Science*, vol. 370, no. 6513, pp. eaba6118, 2020.

[2] L. Barelli, E. Barluzzi, and G. Bidini, "Diagnosis methodology and technique for solid oxide fuel cells: A review", *Int. Journal of hydrogen energy*, vol. 38, no. 12, pp. 5060-5074, 2013.

[3] A. Leonide, S. Hansmann, and E. Ivers-Tiffée, "A 0-dimensional stationary model for anode-supported solid oxide fuel cells", *ECS Transactions*, vol. 28, no. 11, pp. 341, 2010.

[4] M. Sorrentino, P. Cesare, and Y. G. Guezennec, "A hierarchical modeling approach to the simulation and control of planar solid oxide fuel cells", *Journal of Power Sources*, vol. 180, no. 1, pp. 380-392, 2008.

[5] J. Laurencin, D. Kane, G. Delette, J. Deseure, and F. Lefebvre-Joud, "Modelling of solid oxide steam electrolyser: Impact of the operating conditions on hydrogen production", *Journal of Power Sources*, vol. 196, no. 4, pp. 2080–2093, 2011.

[6] A. Saeedmanesh, P. Colombo, D. McLarty, and J. Brouwer, "Dynamic behavior of a solid oxide steam electrolyzer system using transient photovoltaic generated power for renewable hydrogen production", *Journal of Electrochemical Energy Conversion and Storage*, vol. 16, no. 4, pp. 041008, 2019

[7] Y. Bae, S. Lee, K. J. Yoon, J. H. Lee, and J. Hong, "Three-dimensional dynamic modeling and transport analysis of solid oxide fuel cells under electrical load change", *Energy conversion and management*, vol. 165, p. 405-418, 2018.

[8] A. Leonide, Y. Apel, and E. Ivers-Tiffee, "SOFC modeling and parameter identification by means of impedance spectroscopy", *ECS Transactions*, vol. 19, no. 20, pp. 81, 2009.

[9] S. Srikantha, M.P. Heddricha, S. Guptab, K.A. Friedrich, "Transient reversible solid oxide cell reactor operation–Experimentally validated modeling and analysis", *Applied Energy*, vol. 232, pp. 473-488, 2018.

[10] O. B. Rizvandi, and H. L. Frandsen, "Modeling of single-and double-sided high-pressure operation of solid oxide electrolysis stacks", *International Journal of Hydrogen Energy*, 2023.

[11] X. Lin, "A data selection strategy for real-time estimation of battery parameters", *Annual American Control Conference*, pp. 22762281, 2018.

[12] S. Park, D. Kato, Z. Gima, R. Klein, and S. Moura, " Optimal experimental design for parameterization of an electrochemical lithium-ion battery model", *Journal of The Electrochemical Society*, vol. 165, no. 7, pp. A1309, 2018.

[13] Z. T. Gima, D. Kato, R. Klein, and S. Moura, " Analysis of online parameter estimation for electrochemical Li-ion battery models via reduced sensitivity equations," *American Control Conference (ACC)*, pp. 373-378, 2020.

[14] E. B. Poling, J. M. Prausnitz, J. P. O'Connell, *The properties of gases and liquids*, McGraw Hill Professional, 2000.

[15] "NIST Chemistry WebBook, Standard Reference Database 69", 2023, DOI:https://doi.org/10.18434/T4D303.

[16] AKMM Murshed, B. Huang, and K. Nandakumar, "Control relevant modeling of planer solid oxide fuel cell system", *Journal of Power Sources*, vol. 163, no. 2, pp. 830-845, 2007.

[17] F. Monaco, "Analysis of the degradation in solid oxide cells operated in fuel cell and electrolysis modes: microstructural evolution and stability of the electrodes materials", *Doctoral Thesis*, Universite Grenoble Alpes, 2020.

[18] A. J. Bard, L. R. Faulkner, H. S. White, *Electrochemical methods: fundamentals and applications* , Wiley, 1980.

[19] E. N. Fuller, P. D. Schettler, and J. C. Giddings, "New method for prediction of binary gas-phase diffusion coefficients", *Ind. Eng. Chem*, vol. 58, no. 5, pp. 18-27, 1966.

[20] A. Bertei, G. Arcolini, J.P. Ouweltjes, Z. Wuillemin, P. Piccardo, C. Nicolella, " Physically-based deconvolution of impedance spectra: interpretation, fitting and validation of a numerical model for lanthanum strontium cobalt ferrite-based solid oxide fuel cells", *Electrochimica Acta*, vol. 208, pp. 129-141, 2016.

[21] H. Khalil, *Nonlinear systems*, Prentice Hall, 2002.

[22] J. A. Andersson, J. Gillis, G. Horn, J. B. Rawlings, and M. Diehl, "CasADi: a software framework for nonlinear optimization and optimal control", *Mathematical Programming Computation*, vol. 11, pp. 1-36, 2019.

[23] A. C. Hindmarsh, P. N. Brown, K. E. Grant, S. L. Lee, R. Serban, D. E. Shumaker, and C. S. Woodward, "SUNDIALS: Suite of nonlinear and differential/algebraic equation solvers", *ACM Transactions on Mathematical Software (TOMS)*, vol. 31, no. 3, pp. 363–396, 2005.

[24] J. Albicker, " The Gauß-Newton Method and its Implementation in the Optimization Library Oppy", *Master Thesis, Universitat Konstanz, 2022*.